IET The Institution of Engineering and Technology WILEY

**ORIGINAL RESEARCH PAPER**

# Combining electric vehicle battery charging and battery cell equalisation in one circuit

**Huaxia Zhan**[1] | **Haimeng Wu**[2] | **Musbahu Muhammad**[3] | **Simon Lambert**[1] | **Volker Pickert**[1]

[1]School of Engineering, Newcastle University, Newcastle, UK

[2]Department of Mathematics, Physic and Electrical Engineering, Northumbria University, Newcastle, UK

[3]School of Computing, Engineering & Digital Technologies, Teesside University, Middlesbrough, UK

**Correspondence**

Haimeng Wu Department of Mathematics, Physics & Electrical Engineering Ellison Building, Northumbria University, Newcastle upon Tyne, NE1 8ST, United Kingdom.
Email: Haimeng.wu@northumbria.ac.uk

**Abstract**

Electric vehicles (EVs) require an onboard battery charger unit and a battery management system (BMS) unit that balances the voltage levels for each battery cell. So far, both units are two completely autarkic power electronics systems. The circuit presented here operates as a battery charger when the EV is connected to the grid and as a voltage balancer when the EV is driving. Thus, the proposed circuit utilises two functions in one and therefore eliminates the need of having two autarkic units reducing complexity and reduction in component count. The proposed circuit operates as a flyback converter and achieves power factor correction during battery charging. The constant-current constant-voltage (CC–CV) charging method is employed to charge the batteries. However, to limit the number of sensors that will be employed as a result of varying cells during charging, the battery current is estimated using a single current transducer and embedding a converter model in the controller. The operation of the circuit is presented in detail and is supported by simulation results. A laboratory prototype is built to verify the effectiveness of the proposed topology. Experiment results show that the proposed method provides an integrated solution of on-board charging and voltage equalisation.

## 1 | INTRODUCTION

Transportation electrification is an inevitable trend due to the increased global drive towards the adoption of low carbon vehicles to reduce the greenhouse effect. It is projected that for many applications, traditional internal combustion engines (ICEs) will gradually be phased out as a mainstream means of transportation and will be replaced by hybrid and fully electric vehicles in order to reduce $CO_2$ emissions [1, 2]. Most current hybrid electric vehicles (HEVs) and electric vehicles (EVs) are powered by lithium-ion battery packs, which have a high-power density and longer cycle lives compared with other battery technologies [3–5]. In practical applications, each pack is typically made from many battery cells connected in series (or a series-parallel combination) to achieve a higher voltage. However, due to manufacturing tolerances and chemical processes, the specifications of individual cells in a pack vary. After cycling the cells through several charges, voltages between cells can become mismatched. Therefore, a battery management system (BMS) must be employed to actively monitor and balance the voltage across the cells as well as provide safety and longevity [6–14]. Different types of passive and active balancing topologies have been summarised in [15–18]. In addition, onboard battery chargers are required in HEVs/EVs to charge the lithium-ion battery pack. This charger converts AC grid voltage into a controllable DC output voltage to match the state of charge of the battery pack. The current trend by the OEM is to have the BMS and onboard charger as two separate circuits. The equalisation circuit integrated with the transformer commonly requires numerous switches and multiple transformer windings, which has the disadvantages of large volume and expansion difficulty. Many methods of improving the transformer equalisation have been proposed in [19–21], such as a forward-flyback equalisation converter with multi-winding in [19], conventional multi winding topology [20] and half-bridge converters equaliser that reduces the number of windings [21]. However, all the aforementioned configurations add complexity and extra weight to the vehicle, which results in an increased cost and reduced efficiency.

To reduce the complexity, the concept of multi-functional power electronics systems can be applied where only one consolidated circuit is used to conduct battery charging and battery charge equalisation. This concept involves modifying the battery charger to achieve dual functions of charging and battery management. Therefore, eliminating a separate on-board charger unit or the BMS. Several proposals have been published in the literature to include additional functionality in BMS [22, 23]. In [22], a bi-directional battery charger is proposed with a modular integrated equalisation circuit in which the battery cells are connected to the grid via a full-bridge rectifier, a DC/DC converter and a group of switches. The main drawback is that the circuit selects a cell with the lower voltage level and charges it and then terminates the charging process once the maximum voltage threshold is reached. Thus, rather than charging all cells in series simultaneously, each cell is charged individually via the converter. However, once the vehicle is unplugged, no voltage equalisation across the cells can take place due to the chosen circuit topology.

Another study proposes a battery charger that includes a voltage source and a non-dissipative shunt that can be customised to charge any number of batteries [24]. This non-dissipative shunt circuit consists of a pair of transistors and an inductor that is configured as a buck-boost converter to connect with each pair of batteries. In such a configuration, the circuit can be used to charge the battery as a regular EV charger when it is connected to the grid; meanwhile, it is capable of balancing cell voltages through the shunted buck-boost converters when the circuit is unplugged. However, the circuit used for voltage balancing and the circuit used for battery charging does not share any components, and as such, act as two independent circuits having different functions. Therefore, this is not truly a multi-functional power electronics system.

This paper proposes an integrated single stage battery charger/charge equalisation circuit for HEVs/EVs. When the vehicle is static and connected to the grid, the proposed circuit operates as a conventional charger. When the vehicle is operational, that is not connected to the grid; the circuit is controlled to run as a conventional voltage equaliser. The design of such a circuit therefore provides AC/DC conversion, galvanic isolation between the grid and the battery, and charge equalisation. The main contributions of this paper are as follows: (1) Development of single stage charger/charge equalisation circuit using only two winding transformer. (2) Allowing n number of cells to be added by simply modifying the cell selector. (3) Introducing a control structure to improve the overall system performance, flexibility and provide desirable charger/charge equalisation interaction. In addition, the control strategy for charge equalisation is incorporated in the charger control algorithm.

The rest of the paper is organised as follows: Section 2 presents the circuit topology, fundamental operational modes and simulation verification. In Section 3, a control algorithm consisting of a constant-current-constant-voltage (CC-CV) charging algorithm with power factor control (PFC) is proposed and demonstrated. Section 4 describes the validation of the proposed circuit and control algorithms through the construction and operation of a fully functional prototype. Finally, Section 5 summarises the lessons drawn from this work.

## 2 | PROPOSED CIRCUIT TOPOLOGY, OPERATION AND SIMULATIONS

The proposed battery charger integrated with an equalisation circuit is presented in Figure 1. The circuit can be sub-divided into four parts: the rectifier, the isolated converter, the winding selector and the cell selector. For Level 1 unidirectional EV chargers, it is common to add a single-phase full-wave diode bridge rectifier to the grid-side in order to convert AC input into DC [17]. The rectifier is followed directly by an isolated
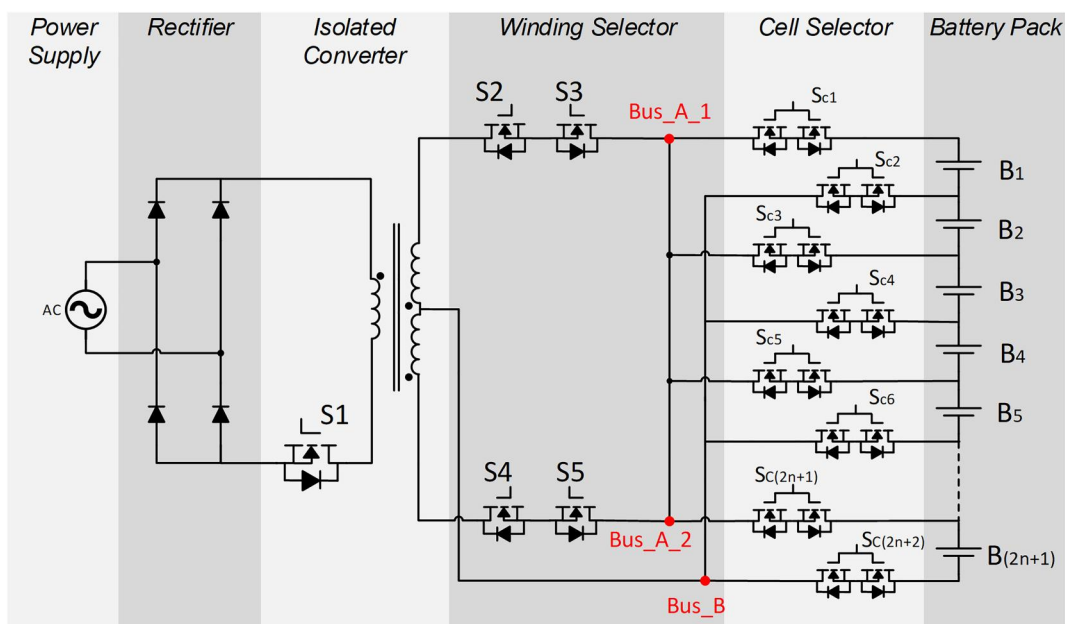


**FIGURE 1** Proposed multi-functional battery charger integrated with voltage equalisation in (2n+1) battery cells

converter, which consists of a three-winding transformer and a transistor that is connected in series to the primary winding. The primary winding and the two secondary windings are reverse-coupled on one magnetic core. Therefore, when power flows from the source to the batteries, irrespective of which secondary winding is involved during the de-magnetizing period, the circuit always works as a flyback converter. Meanwhile, two windings in the secondary side are connected end-to-end. When the energy is transferred between two secondary windings during voltage equalisation, the transformer operates in flyback mode as well. The winding selector comprises two pairs of bi-directional switches that are connected to the top and bottom terminals of the two secondary coils. A bi-directional switch is made up of two anti-series (back-to-back) connected transistors with their body diodes facing opposite directions, and the pair of back-to-back transistors are controlled independently. This arrangement of the winding selector makes it possible that current can go through either of the windings and is under control in both directions.

The cell selector also has a pair of bidirectional switches, which are designed to target the individual battery cells. The positive poles of odd-numbered cells ($B_1$, $B_3$, $B_5$...) are connected to *Bus_A*, and their negative poles are connected to *Bus_B*, while, even-numbered cells ($B_2$, $B_4$...) are connected oppositely. The total number of required bi-directional switches is (n+1) where n stands for the number of cells in the pack. In the cell selector, the two MOSFETs in one bi-directional switch are controlled by a common signal, which can simplify the gate drive circuit. However, this circuit requires the number of cells in a target string to be odd which is to ensure that, when several consecutive cells are charging or discharging together, the top and bottom nodes of the string are connected to *Bus_A* and *Bus_B* separately. For example, $B_1$ can make itself a sink cell by conducting $S_{C1}$ and $S_{C2}$; $B_1$, $B_2$, and $B_3$ together can also be a target by conducting $S_{C1}$ and $S_{C4}$. However, a combination of $B_1$ and $B_2$ may never work because $S_{C1}$ and $S_{C3}$ are both connected to *Bus_A*, and thus there will be no closed current loop from the secondary windings of the isolated converter to the cells.

There are five operational modes for the proposed circuit, including two battery charging modes and three voltage balancing modes. The following section will demonstrate all of the operational modes in detail and will show the corresponding steady-state waveforms. The analysis has been conducted using a five-cell battery pack as an example but would be applicable to any odd-numbered stack length. For the purposes of demonstration of functionality, it is assumed that the MOSFETs are lossless and that the transformer is ideal and perfectly coupled. The battery cell is represented by a large ideal capacitor with a parasitic resistor $R_{cell}$.

## 2.1 | Mode 1: grid charging for odd-numbered cells

The battery charging mode operates in two main periods: a magnetising period and demagnetising period. The operation is
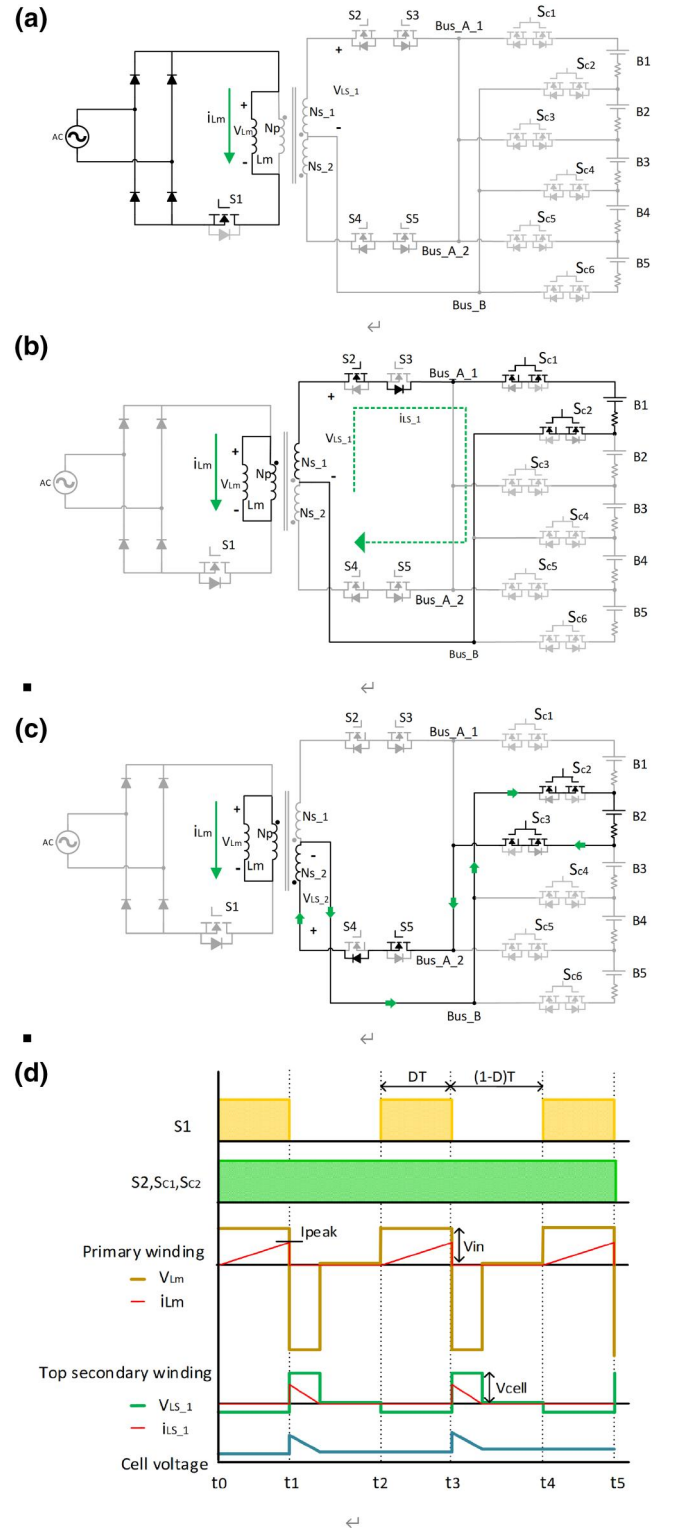


**FIGURE 2** Grid charging: (a) magnetising period; (b) charging for odd-numbered cells; (c) charging for even-numbered cells (d) operational waveforms for charging B1

explained using one odd sink cell $B_1$, but the principle works for all other odd cells. Principal key waveforms for the charging process of $B_1$ are shown in Figure 2 (d).
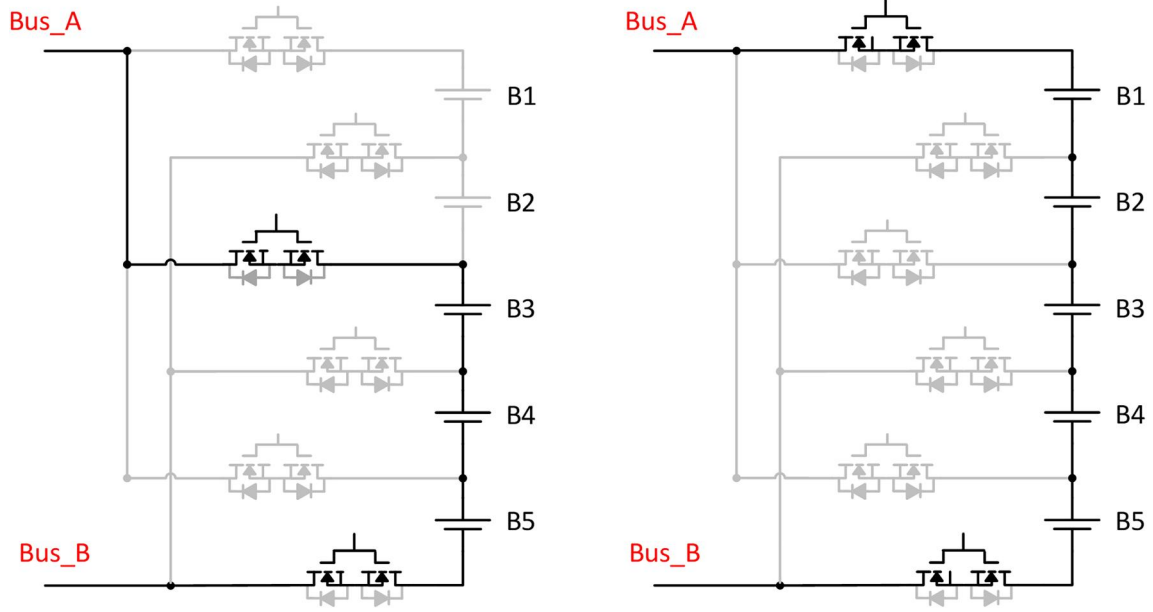
**F I G U R E 3** Examples of battery strings as sink cells

| | Sink Cells | Main Switch | Winding Selector | Cell Selector | |
|---|---|---|---|---|---|
| Mode 1 | $B_{2n-1}$ to $B_{2m-1}$ | $S_1$ | $S_2$ | $S_{C2n-1}$ | $S_{C2m}$ |
| | | PWM | ON | ON | ON |
| Mode 2 | $B_{2n}$ to $B_{2m}$ | $S_1$ | $S_5$ | $S_{C2n}$ | $S_{C2m+1}$ |
| | | PWM | ON | ON | ON |

**T A B L E 1** Cell combination and switching status for mode 1&2

## 2.1.1 | Magnetising period $t_0(t_0 - t_1)$

This period starts when $S_1$ has been turned ON (Figure 2 (a)). During this time, $S_2$ in the winding selector is also ON, and so are $S_{c1}$ and $S_{c2}$ in the cell selector. The current flows from the grid into the primary winding of the transformer. The analysis hereafter assumes that the magnetising inductance $L_m$, is referred to the primary winding. Assuming a switching period $T$ and fixed duty cycle $D$, the current that flows through the primary winding is given as follows:

$$i_{Lm(t)} = \frac{1}{L_m} \int_0^{DT} V_{in} dt \qquad (1)$$

The peak current in the primary winding at the end of the magnetizing period is

$$I_{peak} = \frac{1}{L_m} \cdot V_{in} \cdot DT \qquad (2)$$

## 2.1.2 | Demagnetising period $t_1(t_1 - t_2)$

In the demagnetising period (Figure 2 (b)), $S_1$ is turned off. The energy stored in the transformer is released to the target cell $B_1$ from the secondary winding $N_{s\_1}$ through $S_2$ and the antiparallel diode of $S_3$ in the winding selector, as well as $S_{C1}$ and $S_{C2}$ in the cell selector. The current in $N_{s\_1}$ is gradually decreasing from

$I_{peak}$. If the current reaches zero as the coil magnetomotive force (MMF) has collapsed, $B_1$ will not start discharging because $S_3$ in the winding selector is not turned ON.

The above operation is an example of charging cell $B_1$ only. However, the operation can be applied to any odd-numbered battery cells, or battery strings starting with an odd-numbered cell. Figure 3 shows two examples that multiple cells are charged simultaneously as a battery string. When the sink cells are from *B2n-1* to *B2m-1* (m≥n≥1), the switching states of the MOSFETs involved are shown in Table 1, where PWM means that the device is operating using pulse-width modulation, and ON indicates that the device is fully switched on. Due to the large combination of switching patterns, various charging strategies are possible to optimise the charging speed of the complete battery pack. However, charging optimisation is not the scope of this work and is therefore not further discussed.

## 2.2 | Mode 2: grid charging for even-numbered cells

This operation mode operates identically to Mode 1 except during the demagnetising period; $S_5$, $S_{C2}$, and $S_{C3}$ are conducting, and the current flows from $N_{s\_2}$ through $B_2$, thus charging $B_2$. The equivalent circuit showing the current flow path for charging $B_2$ as an example is shown in Figure 2 (c).
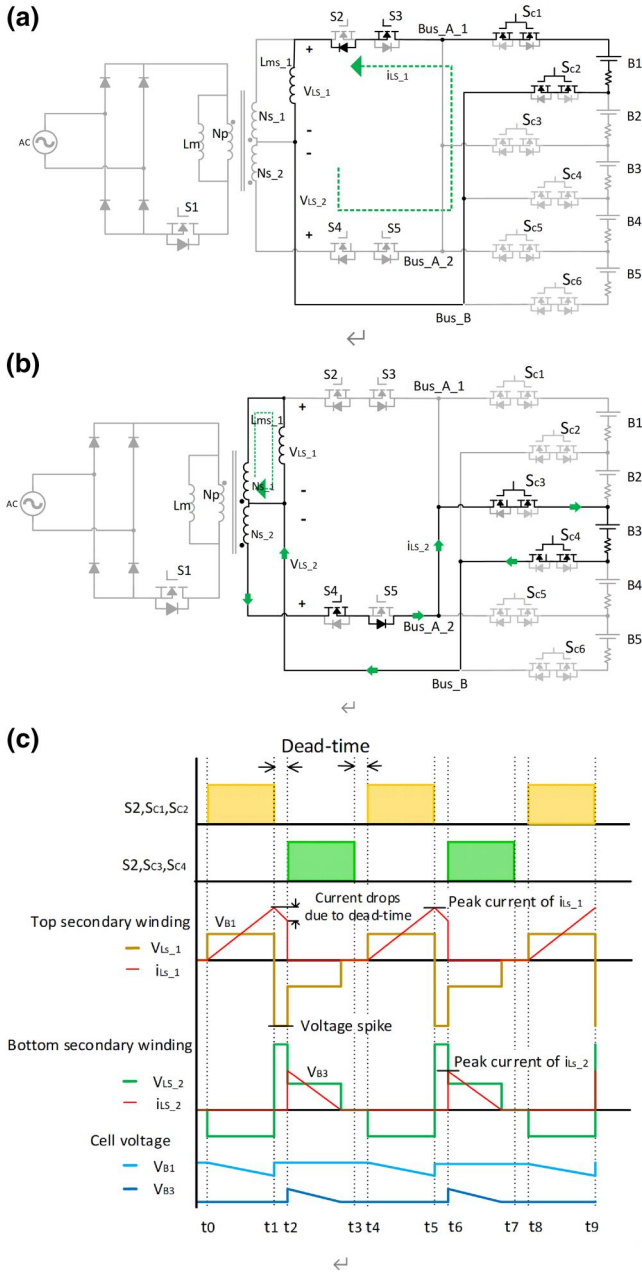
**FIGURE 4** Equalisation from B1 to B3: (a) magnetising period; (b) demagnetising period; (c) key operational waveforms

This operation mode is similar and applicable to all applications as long as the sink cell string starts and ends with even-numbered cells (from $B2n$ to $B2m$, ($m \geq n \geq 1$)), with MOSFETs been switched as shown in Table 1.

## 2.3 | Mode 3: Equalisation from odd cells to odd cells

Here, it is assumed that $B_1$ has a higher initial voltage than $B_3$. An equalisation cycle comprises three sub-intervals: magnetising, dead-time and demagnetising periods. Principal key waveforms for the equalisation are shown in Figure 2(c) and 4(c).

### 2.3.1 | Magnetising period $t_0(t_0 - t_1)$

During this period, $S_{C1}$ and $S_{C2}$ MOSFETs in the cell selector are conducting. Meanwhile, $S_3$ in the winding selector is also turned on, and with the body diode of $S_2$ providing a path for current flow from cell $B_1$ to the secondary winding of the transformer. Thus, energy from $B_1$ is directly transferred into the transformer secondary winding $N_{s\_1}$. In essence, the coil $N_{s\_1}$ serves as an inductive energy storage device. The equivalent circuit for this period is presented in Figure 4 (a)

### 2.3.2 | Dead-time $t_1(t_1 - t_2)$

The overlapping of magnetising and demagnetising period causes short-circuit of the battery cells. For example, if $S_{C3}$ is turned ON before $S_{C1}$ is turned off, $B_1$ and $B_2$ will be shorted via Bus_A. Consequently, a dead-time period must be added between the magnetising and the demagnetising periods for safety. The length of the dead-time period depends on the switching characteristics of the MOSFETs. In this paper, dead-time in both simulations and experimental tests are set to 1 µs.

### 2.3.3 | Demagnetising period $t_2(t_2 - t_3)$

The energy stored in the transformer secondary winding $N_{s\_1}$ is now released to the sink battery $B_3$. $S_4$ in the winding selector and $S_{C3}$, $S_{C4}$ in the cell selector are gated ON, so that a demagnetising current $i_{Ls\_2}$ can flow from the bottom secondary winding $N_{s\_2}$ through $S_4$ and the body diode of $S_5$, and $S_{C3}$ to the sink cell. The equivalent circuit of this period is shown in Figure 4 (b).

It is important to ensure that the demagnetising current falls back to zero before the subsequent magnetising period begins. Otherwise, the flux in the transformer will build up over every switching event, which will cause saturation of the magnetic core. The duty cycle of the pulse signal determines whether the demagnetising current will return to zero in time. The following equations can be obtained as follows:

$$I_{Ls\_1\_peak} = \frac{V_{B1} \times DT}{L_{ms\_1}} \quad (3)$$

$$V_{B3} = L_{ms\_1} \times \frac{I_{Ls\_1\_peak}}{(1-D)T} \quad (4)$$

Substituting (3) into (4), the critical value of $D$ in the steady state can be derived as

$$D_c = \frac{V_{B3}}{V_{B1} + V_{B3}} = \frac{1}{\frac{V_{B1}}{V_{B3}} + 1} \quad (5)$$

Equation (5) shows that the critical duty cycle is determined by the voltages of both the source and sink cells in the
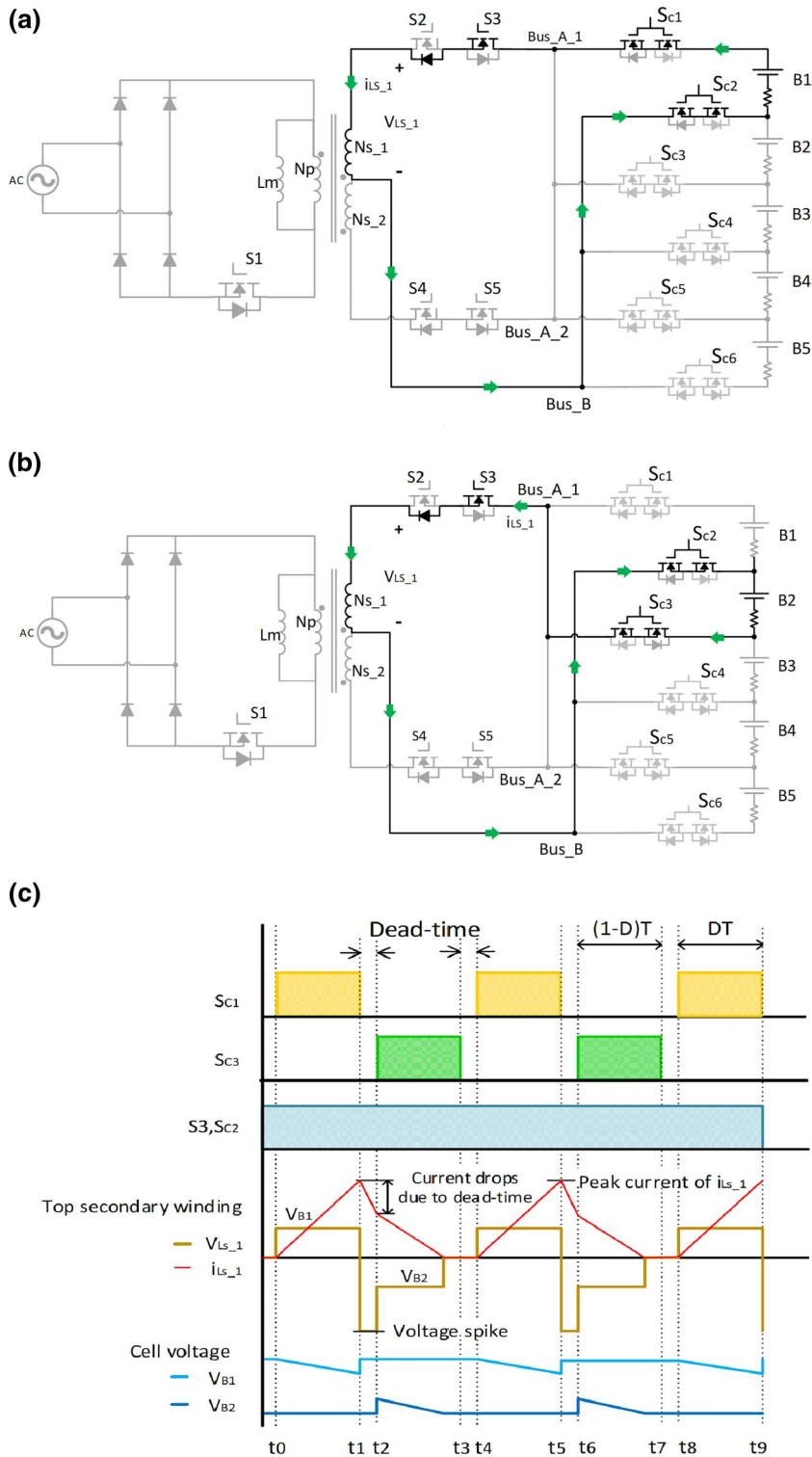
**(a)**

**(b)**

**(c)**

steady state when both the source and the target are single cells, thus, the bigger the voltage difference between them, the smaller is the required duty cycle. This conclusion can be used to develop a control algorithm for battery equalisation, which generates PWM signals, which are a function of the voltages of the source and sink cells.

This operating mode is an illustration of the transfer of energy from $B_1$ to $B_3$. However, the model applies for voltage equalisation between all odd-numbered cells (or strings that start with an odd cell). Combination of the source cells and the sink cells and the corresponding switching status are listed in Table 2.

## 2.4 | Mode 4: Equalisation from even cells to even cells

This mode has the same operating principle as Mode 3. The source cells and the sink cells are involved in this mode and the corresponding switching status is presented in Table 2.

## 2.5 | Mode 5: Equalisation between odd cells and even cells

Unlike the previous four operational modes in which the circuit operates as a flyback converter, in Mode 5, the circuit operates as a buck-boost converter. Furthermore, since there is only one secondary coil involved (other coils are open circuit), it is

considered as a single coil inductor rather than being coupled to other windings. The balancing process can also be divided into three periods: the inductor charging period, the dead-time, and the inductor discharging period. Principal key waveforms for the equalisation are shown in Figure 2(c) and 5(c).

### 2.5.1 | Inductor charging period $t_0(t_0 - t_1)$

During this time, $B_1$ is connected to the top secondary winding $N_{s\_1}$ with $S_{C1}$ and $S_{C2}$ in the cell selector gated ON (Figure 2(a) and 5(a)). $S_3$ in the winding selector is also conducting to provide a current flow path from $B_1$ to charge the transformer winding $N_{s\_1}$. Within this period, the coil is storing magnetic energy in the transformer core.

**TABLE 2** Cell combination and switching status for mode 3,4 and 5

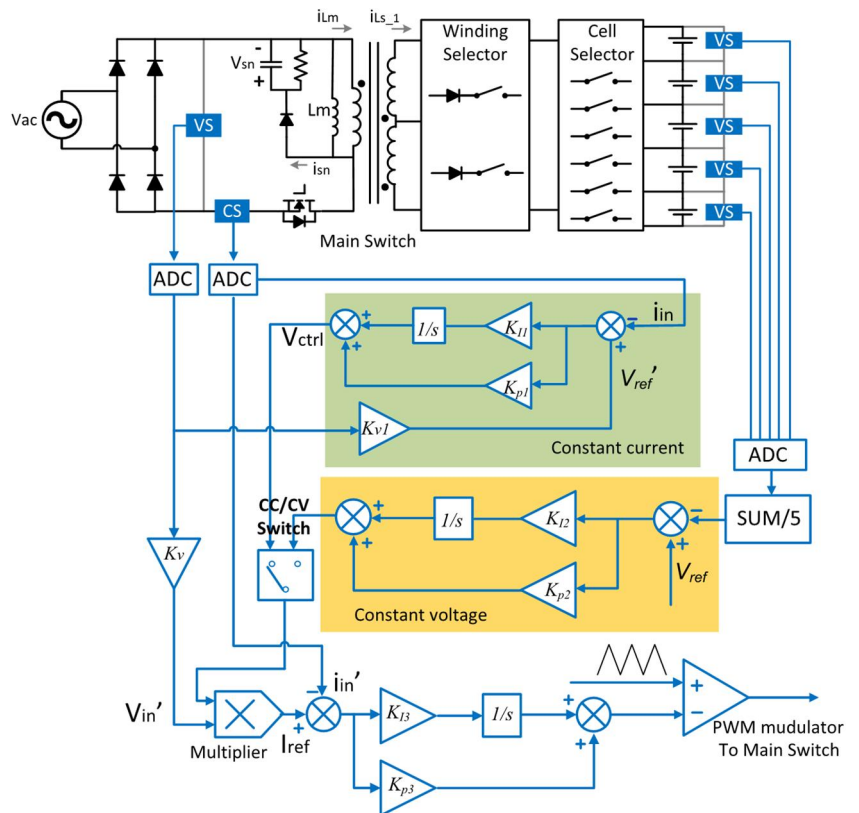| | Source Cells | Sink Cells | Magnetizing | De-magnetizing |
|---|---|---|---|---|
| Mode 3 | $B_{2n-1}$ to $B_{2m-1}$ | $B_{2k-1}$ to $B_{2p-1}$ | $S_3$, $S_{C2n-1}$, $S_{C2m}$ | $S_4$, $S_{C2k-1}$, $S_{C2p}$ |
| | | | ON | ON |
| Mode 4 | $B_{2n}$ to $B_{2m}$ | $B_{2k}$ to $B_{2p}$ | $S_4$, $S_{C2n}$, $S_{C2m+1}$ | $S_4$, $S_{C2k}$, $S_{C2p+1}$ |
| | | | ON | ON |
| Mode 5 | $B_{2n-1}$ to $B_{2m-1}$ | $B_{2k}$ to $B_{2p}$ | $S_3$, $S_{C2n-1}$, $S_{C2m}$ | $S_3$, $S_{C2k}$, $S_{C2p+1}$ |
| | | | ON | ON |
| Mode 5 | $B_{2n}$ to $B_{2m}$ | $B_{2k-1}$ to $B_{2p-1}$ | $S_2$, $S_{C2n}$, $S_{C2m+1}$ | $S_2$, $S_{C2k-1}$, $S_{C2p}$ |
| | | | ON | ON |



**FIGURE 6** Diagram of the proposed circuit with the power factor control-CC-CV controller

## 2.5.2 | Dead-time $t_1(t_1 - t_2)$

As mentioned previously, any overlap of the conducting of MOSFETS may have an impact on the battery cells and transistors. This is also true in this operation mode; hence, a dead-time is necessary. At time $t_1$, the cell selector, $S_{C1}$, is switched off.

## 2.5.3 | Inductor discharging period $t_2(t_2 - t_3)$

At $t_2$, $S_{C3}$ is switched ON, $S_3$ continues to conduct, and therefore the sink cell $B_2$ is in series with the secondary winding $N_{s\_1}$ (Figure 2(b) and 5(b)). Thus, the energy stored in the core is released to $B_2$. Although it is not essential for the converter to operate in discontinuous conduction mode (DCM) for this operating mode –providing the next period is in the same operating mode–when moving between modes the core must be demagnetised, the assumption is that the converter is operated in DCM. Thus, the critical duty cycle shown in Equation (5) can be applied to this operating mode. The source cells and sink cells involved as well as the corresponding switching states in this mode are also included in Table 2.

Thus, to cope with the imbalance of multiple cells, the proposed circuit can operate as a mains charger and only to charge the cells that have lower voltage. Alternatively, the circuit can operate as an equaliser, using cells that have higher voltage to charge the rest cells. In other words, the proposed circuit can balance the voltage across the cells in two ways: voltage balancing as a charger and voltage balancing as an equaliser. When the circuit is connected to a power supply, it can choose the target cell/cells with the winding selector and the cell selector working together. Hence, cell/cells with higher voltage would be bypassed, and cell/cells with lower voltage can be charged. In this way, the voltage difference between cells will be reduced. The combinations of target cell/cells have been demonstrated in Table 1 in the paper. The circuit can also balance the voltage as an equalisation circuit. It can operate as either flyback converter-based equaliser, or buck-boost converter-based equaliser. Section 2.3, 2.4 and 2.5 in the paper gave examples for the three equalisation operational modes, which demonstrate that energy can be transferred from one cell to another in the pack, with the winding selector and the cell selector working together. Furthermore, the source and target can be a cell string, and the combinations of the cells have been shown in Table 2.

# 3 | PFC & CC-CV CONTROLLER FOR THE PROPOSED CIRCUIT

To comply with the IEEE and the Society of Automotive Engineers (SAE) standards, it is a common practice to include a power factor correction (PFC) circuit for onboard battery chargers when they are connected to the power grid [25–28]. As the proposed circuit operates as a flyback converter during battery charging, one significant advantage of the proposed

**TABLE 3** Key parameters in the simulation model

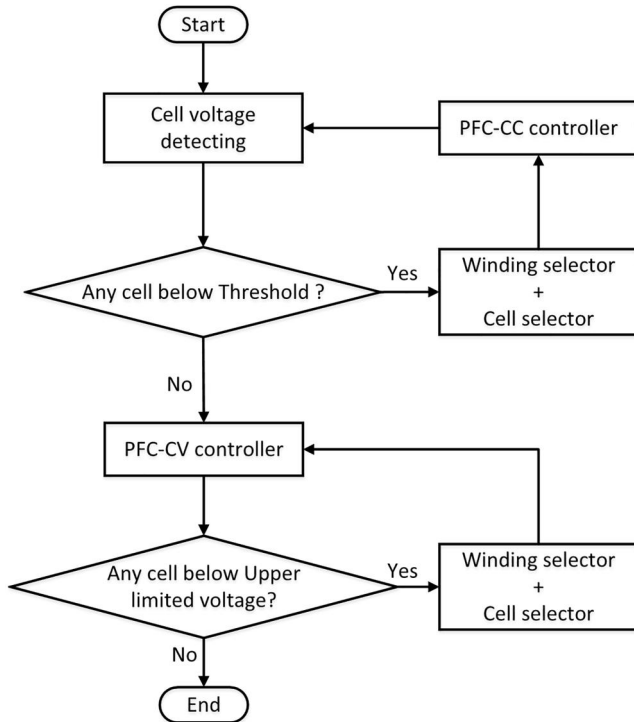| Parameters | Values |
| --- | --- |
| Power Input | 230 V AC, 50 Hz |
| Transformer's Turns Ratio | 11:1 |
| Magnetic Inductance Lm | 350 uH |
| Cells' Capacitance | 200 F |
| Cells' Resistance | 0.011 Ω |



**FIGURE 7** Flow chart of the proposed control algorithm
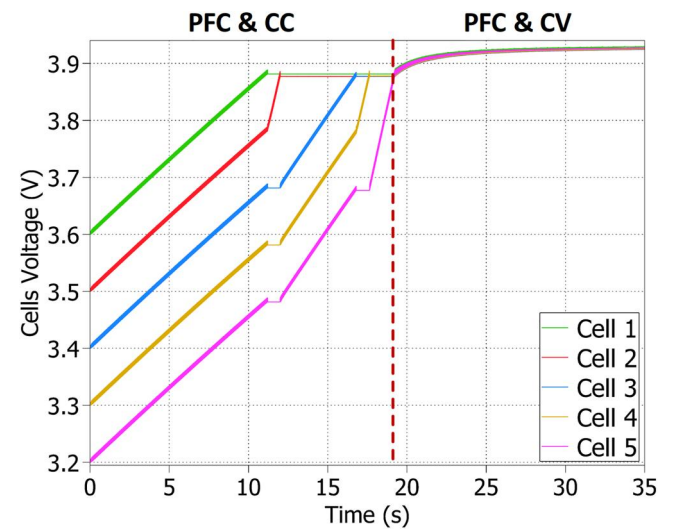


**FIGURE 8** Simulation results of battery charging with power factor control-CC-CV controller

topology is the capability of achieving PFC without using additional inductors, diodes or switches.

Figure 6 shows the diagram of the proposed circuit with the PFC-constant current (CC) and constant voltage (CV) controller. The controller consists of four functional blocks: the outer voltage loop, the outer current loop, the inner current loop, and the PWM modulator.

It is a common practice to charge batteries using a CC-CV format whereby in the early stage of battery charging when cell voltages are far below the maximum allowable cell voltage, a CC is applied (at the desired C-rate). Figure 6 also shows the

PFC-CC control mode for the proposed circuit. In CC mode, the charging current could be measured from the secondary side; however, since the topology allows varied numbers of cells to be charged, placing the current transducer on the secondary side may not be optimal. Instead, by using the primary side current transducer combined with the knowledge of the transformer turns ratio, as well as the number of cells being charged, the secondary current can be estimated through embedding a converter model in the controller. In this way, only one primary current sensor is required for the entire system control. The outer control loop regulating the current level and the inner loop
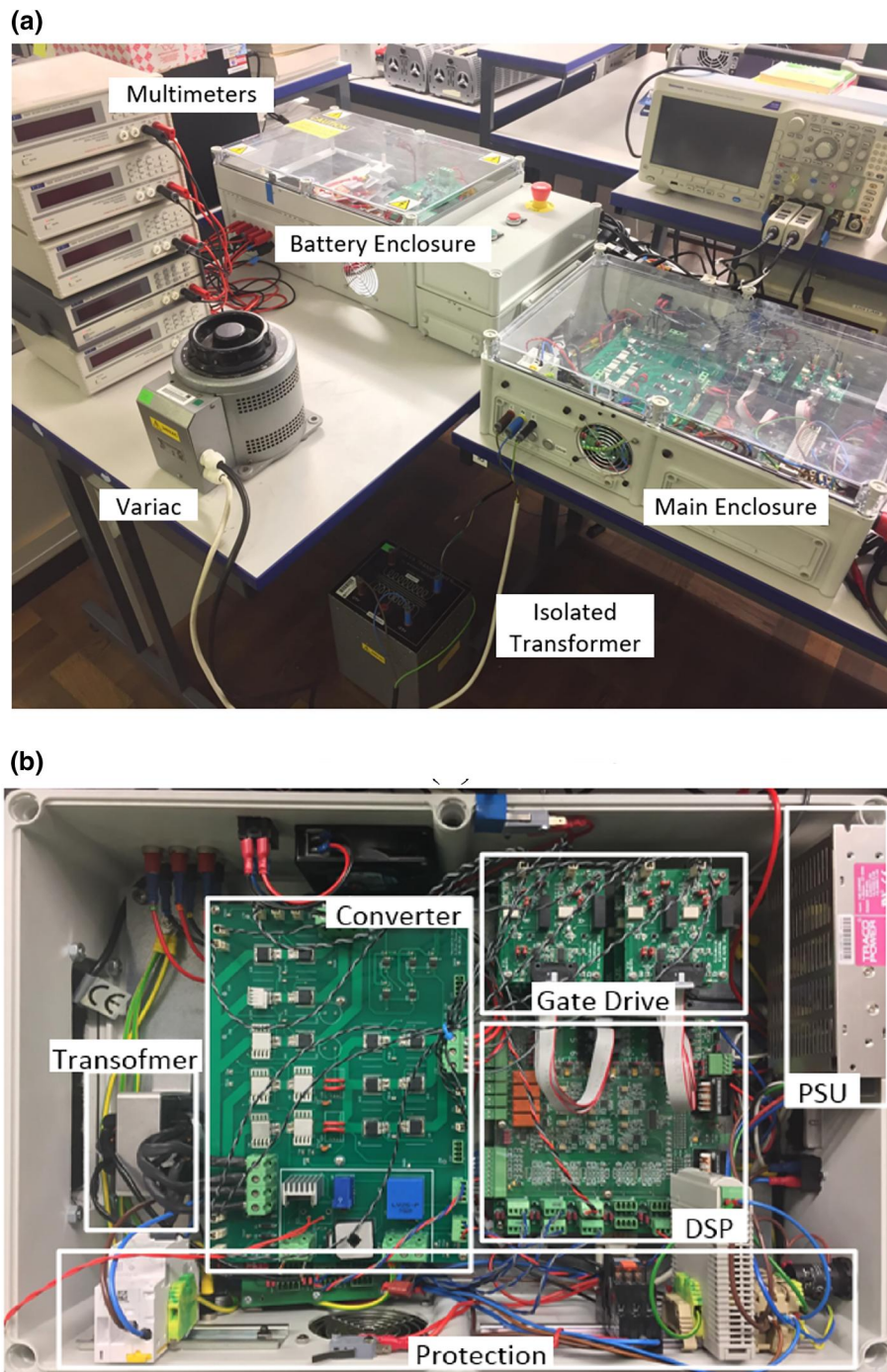


**FIGURE 9**  Photos (a) test bench; (b) prototype converter

regulating the current envelope means the controller keeps the circuit at the CC output with a high input power factor.

The outer voltage loop aims to compare the circuit output voltage with a voltage reference before regulating the voltage

error. Therefore, this controller is also regarded as the PFC-CV controller, and it can be used in the later stage of battery charging when cell voltages approach the upper voltage limit, and CV charging is demanded [29–31].

The voltages of each cell are measured, and an averaged value $V_0$ is calculated as the output voltage of the system. Since, as set by the control algorithm, the number of cells in the charging state is determined by the status of cells and the fully charged cells will be bypassed in the circuit. Thus, using the average voltage instead of the overall output voltage allows adaptation to the reference in the outer voltage loop. In this way, the reference can be set as the upper voltage limit of one battery cells no matter how many cells are charging. The average voltage is compared with the battery stack reference voltage $V_{ref}$, producing the control signal $V_{ctrl}$, which is multiplied by the regulated input voltage $V'_{in}$. Thus, the current reference $I_{ref}$ contains the information of the envelope and the generated DC components of the battery pack. In the inner current loop, $I_{ref}$ is compared with the regulated current $i'_{in}$ and the error is controlled by the current loop PI controller. The

**TABLE 4** Specification of key components used in the prototype

| Part | Model |
| --- | --- |
| Rectifier | Fairchild, GBPC2504W |
| S1 | CREE, C2M0080120D |
| $S_2$-$S_5$, $S_{C1}$-$S_{C6}$ | ON, AUIRFS8409-7P |
| Zener Diode | On, 1N5364BG |
| Voltage Hall Sensor | LEM, LV25-P |
| Current Hall sensor | LEM, CAS 6-NP |
| Differential Amp | AD, AD629 |
| DSP | Texas Instruments TMS320F28335 |

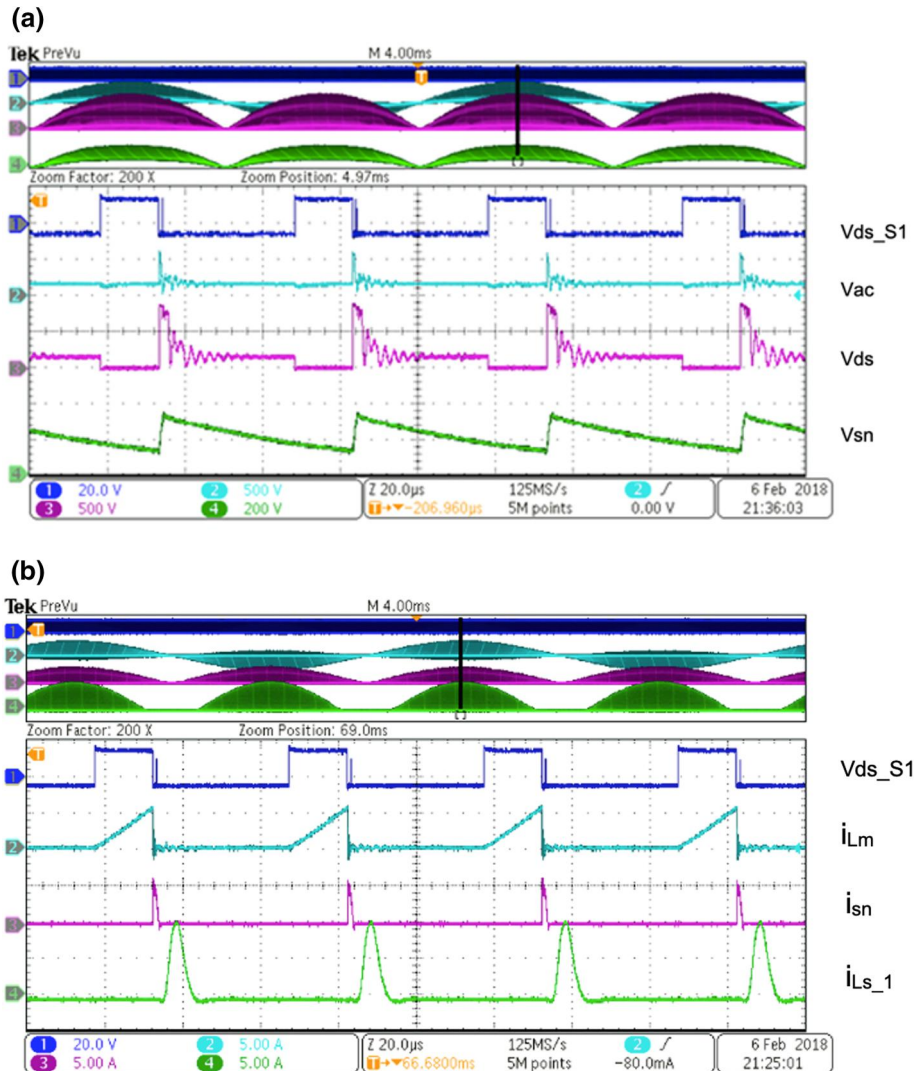Abbreviation: DSP, digital signal processor.



**FIGURE 10** Experimental results when charging five cells: (a) voltage waveforms; (b) current waveforms

controlled signal is then fed into a PWM modulator to drive the *S1* in the circuit.

The flow chart of the proposed control algorithm is presented in Figure 7. The cells voltages are first measured to determine the controller whether to run in the PFC-CC or PFC-CV mode. If the voltage of any cell is under the threshold voltage, the PFC-CC controller is activated, charging the batteries at the desired C-rate. The winding selector and cells selector will work together to bypass cells that reach the threshold voltage. Once all the cells reach the threshold voltage, the controller is switched to the PFC-CV control mode to charge the cells with a decreased charging current. When individual cells reach the upper voltage limit, the winding selector and cells selector will work together to bypass the fully charged cells and make the converter to charge the rest of the cells. Thus, in time, all the cells can be charged to the same upper voltage limit. There is necessarily a hysteresis around the CC-CV decision point to avoid the controller losing stability at the threshold.

The proposed circuit and the controller have been simulated using the software PLECS. The parameters in the simulation model are presented in Table 3.

Figure 8 shows the input current and cell voltages of a complete simulated PFC-CC-CV charge process of five cells. In this simulation, it was assumed that five cells have different initial voltage from 3.2 to 3.6 V. To save the simulation time, the capacitance values of the cells are reduced to 200 F. Based on this scenario, the threshold voltage for each cell and the upper voltage limit are set at 3.88 and 3.93 V, respectively. All the five cells are charged simultaneously in the first stage of PFC-CC charging. It can be seen that B1 first reaches the threshold voltage and it is bypassed. Since the number of cells in the target string has to be odd, the rest of four cells cannot be charged together. Hence, B2 is charged alone in the next stage.

Then, B3, B4 and B5 are charged in series until B3 reaches the threshold. In the following stage, B4 and B5 are charged in turn for a short period. When all the five cells reach the threshold voltage, the controller switched from CC to CV charging. It is evident that the charging speed slows down when in CV mode.

# 4 | EXPERIMENTAL TESTS AND OPERATIONAL MEASUREMENTS

A prototype converter has been built and tested to verify the performance of the proposed circuit and the control algorithm. Figure 9 (a) shows a photo of the test bench and Figure 9 (b) presents the photo of the prototype system containing the power converter, DSP controller and the gate drives. The output of the converter is connected to a battery enclosure, which contains the battery pack and protection circuits. The specification of the key components used in the prototype is
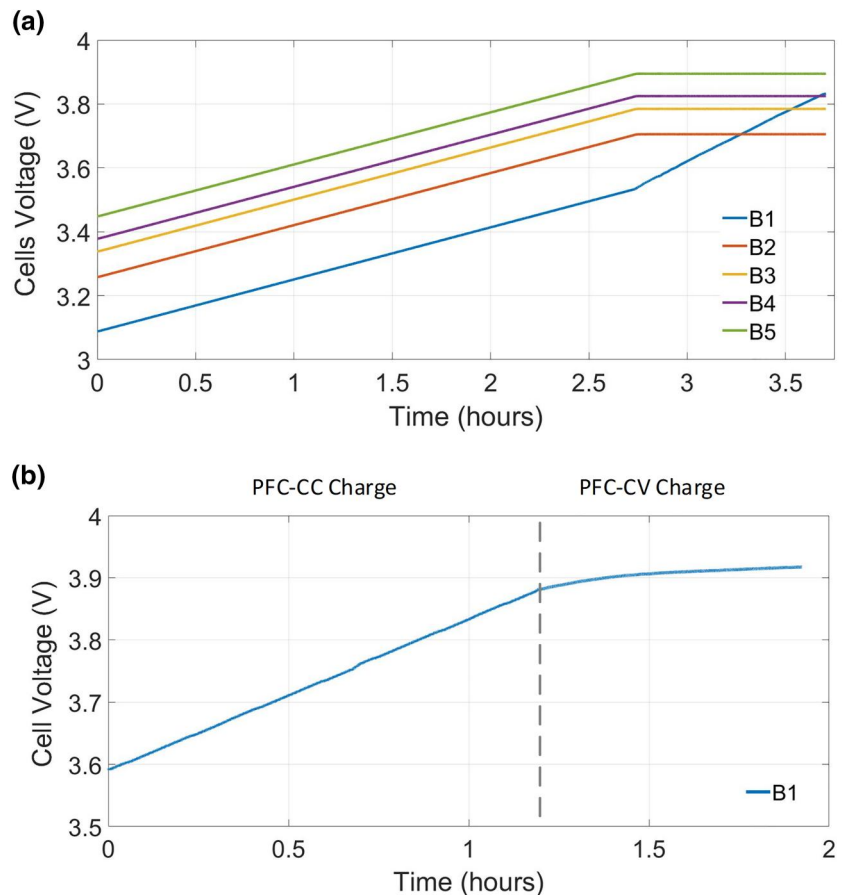


**FIGURE 11** Cells voltages during charging under (a) open-loop control; (b) power factor control-CC control

presented in Table 4. During battery charging, the energy stored in the leakage inductor can cause a voltage spike that increases the voltage stress on the power MOSFET switches, thus, to suppress the voltage spike, an RCD snubber circuit is used across the primary winding.

As the circuit provides numerous combinations, only a few operations can be presented. For charging, two scenarios have been selected. Scenario one is the PFC-CC charging of 5 cells switching from 5 cells charging to 1 cell charging, and Scenario two is charging one cell switching from PFC-CC charging to PFC-CV charging. Likewise, for balancing, two scenarios have been selected. Scenario one is balancing from an odd-numbered cell to an odd-numbered cell, and Scenario two is balancing from an odd-numbered cell to an even-numbered cell.

Figure 10 shows the measured waveforms for the circuit in operation as a battery charger with the input voltage of 100 Vac RMS, 50 Hz, and the switching frequency of 20 kHz. The input voltage $V_{ac}$, the voltage across $S_1$ $V_{ds}$, and the voltage across the snubber circuit $V_{sn}$ are shown in Figure 10 (a). Figure 10 (b) presents the current waveforms, including the current through the primary winding of the transformer $i_{Lm}$, the current through the first secondary winding $i_{Ls\_1}$ and the current flowing into the snubber circuit $i_{sn}$. Figure 11 shows the voltage oscillations of $V_{ds}$ and a reduced current on the secondary winding compared with the input current on the

primary winding. This is due to the leakage inductance of the transformer used in this circuit

Figure 11 (a) illustrates an example of charging five and one cell during CC mode. The initial voltages of $B_1$ to $B_5$ are set to 3.08 , 3.25, 3.33, 3.37 and 3.44 V, respectively. In the first stage, all five cells are in CC charging mode and the cell voltages increases.

After being charged for about 2 h and 40 min, all battery cells passed the lower threshold voltage of 3.7 V except $B_1$. At this point, $B_1$ to $B_4$ are bypassed, meaning these cells are not further charged. Consequently, more energy can now be transferred into $B_5$, which increases the charging speed for this cell. At approximately 3.8 h, the charging process is completed. It is worth noting that, in contrast to the simulation result in Figure 8, there is a charge difference of about 100 mV between the cells (i.e. B1-B4). Such kind of voltage differences among cells are normally caused by cell imbalances and a change in internal resistance. In addition, issues such as sampling rate of the ADC and manufacturing tolerances always playout. Furthermore, all the cells were assumed to have 200 F during simulation.

Figure 11 (b) shows the charging process of one cell $B_1$ when it is charged under the PFC-CC and PFC-CV control, respectively. In the first 1.2 h, PFC-CC control is applied, and the voltage of $B_1$ rises linearly from an initial voltage of 3.55 to
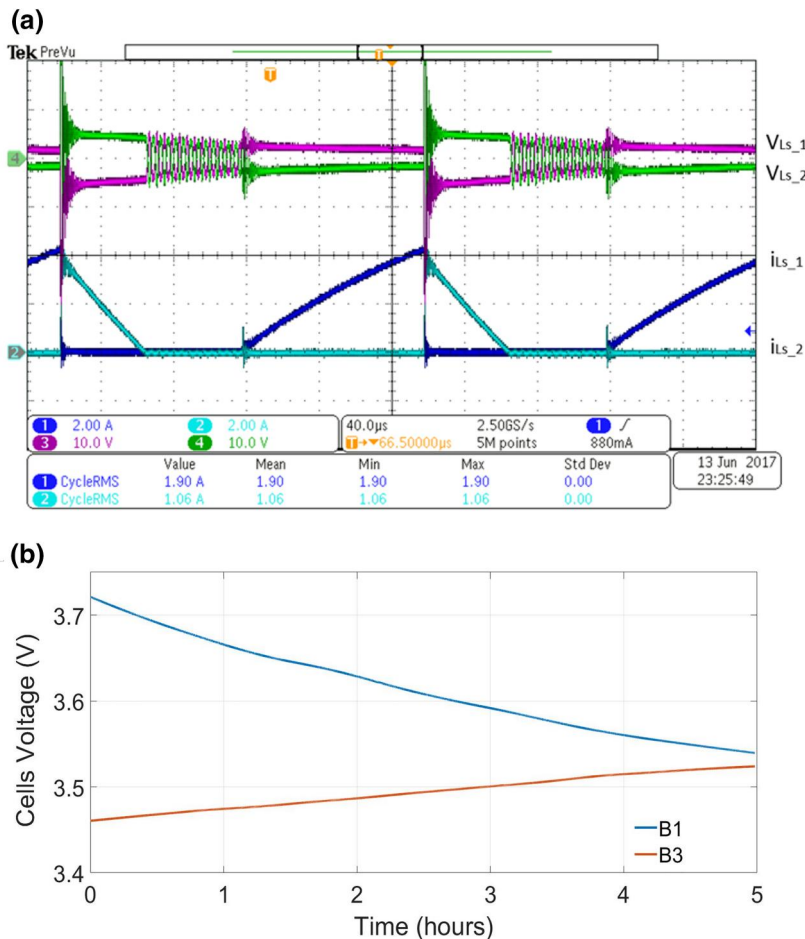


**FIGURE 12** Waveforms of voltage equalisation from $B_1$ to $B_3$: (a) voltage and current in the converter; (b) cells voltage

3.85 V. In the second period, the controller is switched to PFC-CV control, so that the charging speed in this period slows down and the voltage of $B_1$ reaches 3.9 V at the end after about another two hours charging.

The performance of voltage equalisation has been tested between odd-numbered cells, which is between the source cell $B_1$ and the sink cell $B_3$, with the switching frequency of 5 kHz. The initial voltages of $B_1$ and $B_3$ are set at 3.7 and 3.44 V, respectively. The operational waveforms of voltages and currents during the equalisation process are shown in Figure 12 (a), from bottom to top, they are the discharging current of $B_1$ ($i_{LS\_1}$), the charging current of $B_3$ ($i_{LS\_2}$), the voltage across the winding $Ns\_1$ ($VLS\_1$), and the voltage across the winding $Ns\_2$ ($VLS\_2$), respectively. Figure 12 (b) shows the process of cell voltage of $B_1$ and $B_3$ approaching a balanced voltage of about 3.53 V.

Figure 13 presents the key operational waveforms and cell voltages changes to demonstrate the voltage equalisation between an odd-numbered cell and an even-numbered cell. In this test, voltage equalisation is between the source cell $B_1$ and the sink cell $B_2$ and the cells in the pack are pre-charged to initial states where $B_1$ is at 3.8 V, $B_2$ is at 3.25 V.

The measured waveforms from top to bottom in Figure 13 (a) are gate signal of $S_{C1}$, the voltage of $B_1$ ($V_{B1}$), the voltage of $B_2$ ($V_{B2}$), and the current through the winding $N_{s\_1}$ ($iLS\_1$).

As it can be seen, there is a drop in the current magnitude after MOSFET $S_{C1}$ has been turned off. This is due to the dead-time between the turning off of $S_{C1}$ and the turning ON of $S_{C3}$ to protect the cells $B_1$ and $B_2$ from short circuit. Figure 13 (b) shows the cells' voltage during the equalisation process. It is evident that a balanced voltage between $B_1$ and $B_2$ has been achieved at about 3.4 V for both cells.

The four different examples show that the proposed circuit has two different functions. It allows battery charging and cell equalisation by using the same circuit components. Therefore, the proposed circuit is an alternative to today's technology where electric vehicles use one power electronics circuit for charging and another circuit for battery cell equalisation.

## 5 | CONCLUSION

The battery charging system of EVs typically requires two independent units to achieve a grid-connected charging process and voltage equalisation of battery cells with increased cost, weight and volume. This paper presents a circuit topology that can be used as both a grid charger and a cell voltage equaliser in a single circuit. When the vehicle is static and connected to the grid, the proposed power circuit operates as
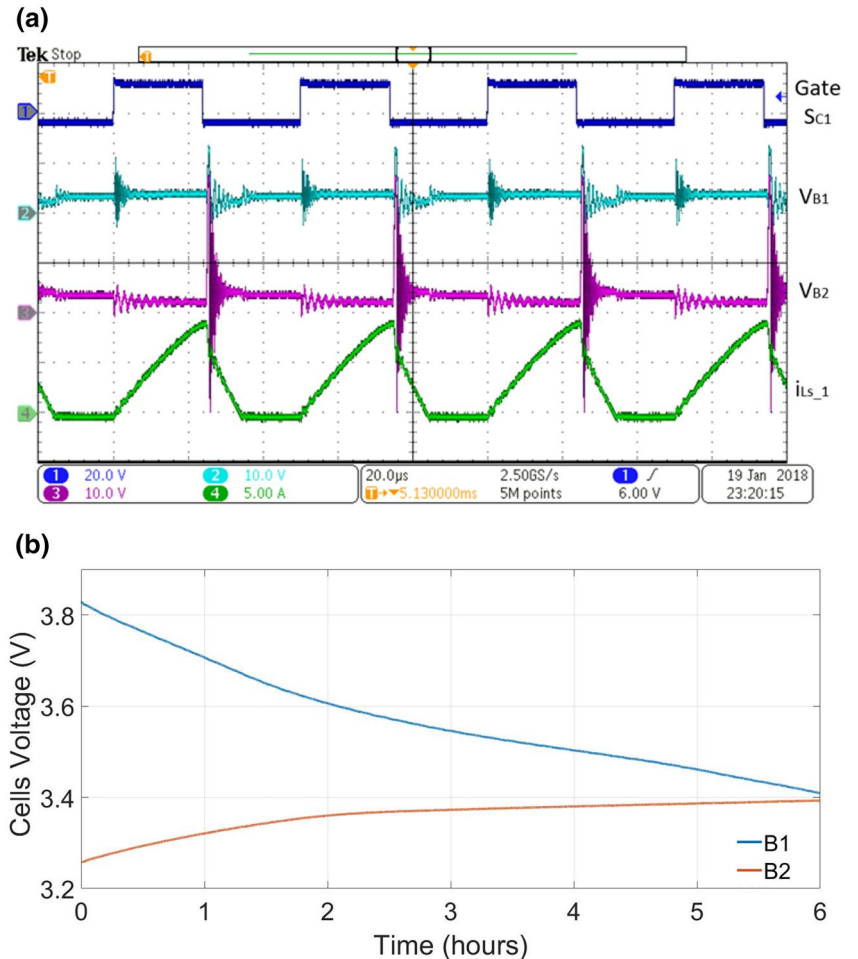


**FIGURE 13** Waveforms of voltage equalisation from $B_1$ to $B_2$: (a) voltage and current in the converter; (b) cells voltage

an onboard charger with functional blocks including AC/DC conversion, PFC and isolated DC/DC conversion. When the vehicle is not connected to the grid, and unbalanced voltage is detected within the battery pack, the proposed circuit operates as a standalone equaliser. The operational principle of the proposed circuit is discussed. Selected experimental results are shown to validate the effectiveness of the proposed circuit.

## ORCID

*Haimeng Wu* 🆔 https://orcid.org/0000-0002-6613-9908

## REFERENCES

1. https://www.epa.gov/ghgemissions/overview-greenhouse-gases, (2017)
2. https://www.gov.uk/government/statistics/provisional-uk-greenhouse-gas-emissions-national-statistics-2016, (2017)
3. Khaligh, A., et al.: Battery, ultracapacitor, fuel cell, and hybrid energy storage systems for electric, hybrid electric, fuel cell, and plug-in hybrid electric vehicles: state of the art. IEEE Trans. Veh. Technol. 59. 2806–2814 (2010)
4. Lu, L., et al.: A review on the key issues for lithium-ion battery management in electric vehicles. J Power. Sources. 226, 272–288 (2013)
5. Burke, A.F.: Batteries and ultracapacitors for electric, hybrid, and fuel cell vehicles. Proc. IEEE. 95(4), 806–820 (2007)
6. Cheng, K.W.E. et al.: Battery-management system (Bms) and soc development for electrical vehicles. IEEE Trans. Veh. Technol. 60(1), 76–88 (2010)
7. Lambert, S., et al.: Overview of supercapacitor voltage equalisation circuits for an electric vehicle charging application. In: IEEE Vehicle Power and Propulsion Conference. IEEE (2010)
8. Barrade, P.: Series connection of supercapacitors: comparative study of solutions for the active equalisation of the voltages. In: Proceedings of 7th International Conference on Modelling and Simulation of Electric Machines. Converters and Systems (2002)
9. Lambert, S.M., et al.: Transformer-Based equalisation circuit applied to N-number of high capacitance cells. IEEE Trans Power Electron. 31(2), 1334–1343 (2015)
10. Zhan, H., et al.: A Cascaded Transformer-Based Equalisation Converter for Series Connected Battery Cells. In: 8th IET International Conference on Power Electronics, Machines and Drives (PEMD 2016) (2016)
11. Wu, H., et al.: A ripple reduction method for a two stages battery charger with multi-winding transformer using notch filter. In: Power Electronics and Drive Systems (PEDS), 2017 IEEE 12th International Conference on. IEEE (2017)
12. Khaligh, A., Dusmez, S.: Comprehensive topological analysis of conductive and inductive charging solutions for plug-in electric vehicles. IEEE Trans. Veh. Technol. 61(8), 3475–3489 (2012)
13. Duan, C., et al.: A solar power-assisted battery balancing system for electric vehicles. IEEE Trans. Transport. Electrification. 4(2), 432–443 (2018)
14. Frost, D.F., Howey, D.A.: Completely decentralised active balancing battery management system. IEEE Trans. Power Electron. 33(1), 729–738 (2017)
15. Hsieh, Y.H., et al.: A novel high-efficiency compact-size low-cost balancing method for series-connected battery applications. IEEE Trans. Power Electron. 28(12), 5927–5939 (2013)
16. Moore, S.W., Schneider, P.J.: A Review of Cell Equalisation methods for Lithium Ion and Lithium Polymer Battery Systems. SAE Technical Paper (2001)
17. Cao, J., Schofield, N., Emadi, A.: Battery balancing methods: A comprehensive review. In: IEEE Vehicle Power and Propulsion Conference. IEEE (2008)
18. Nazi, H., Babaei, E., Sabahi, M.: Bidirectional active charge equaliser for series-connected cells. IET Power Electron. 12(5), 1229–1240 (2019)
19. Shang, Y., et al.: An automatic equaliser based on forward-flyback converter for series-connected battery strings. IEEE Trans. Ind. Electron. 64(7), 5380–5391 (2017)
20. Li, S., Mi, C.C., Zhang, M.: A high-efficiency active battery-balancing circuit using multiwinding transformer. IEEE Trans. Ind. Appl. 49(1), 198–207 (2013)
21. Shang, Y., Cui, N., Zhang, C.: An optimised any-cell-to-any-cell equaliser based on coupled half-bridge converters for series-connected battery strings. IEEE Trans. Power Electron. 34(9), 8831–8841 (2019)
22. Tashakor, N., Farjah, E., Ghanbari, T.: A bidirectional battery charger with modular integrated charge equalisation circuit. IEEE Trans. Power Electron. 32(3), 2133–2145 (2016)
23. Brainard, G.L.: Non-dissipative Battery Charger Equaliser. Google Patents (1995)
24. Chiang, R., Lu, K., Huang, J.: Intelligent Equalising Battery Charger Having Equalisation Charging Circuitry. Google Patents (2009)
25. Yilmaz, M., Krein, P.T.: Review of battery charger topologies, charging power levels, and infrastructure for plug-in electric and hybrid vehicles. IEEE Trans. Power Electron. 28(5), 2151–2169 (2012)
26. Abdel-Rahman, S., Stückler, F., Siu, K.: Pfc Boost Converter Design Guide 1200 W Design Example. Application Note (2016)
27. Zhang, J., Lu, D.D.C., Sun, T.: Flyback-Based single-stage power-factor-correction scheme with time-multiplexing control. IEEE Trans. Ind. Electron. 57(3), 1041–1049 (2009)
28. Jiang, Y., Lee, F.C.: Single-Stage single-phase parallel power factor correction scheme. In: Proceedings of 1994 Power Electronics Specialist Conference-PESC. 94. IEEE (1994)
29. Chen, B.-Y., Lai, Y.-S.: New digital-controlled technique for battery charger with constant current and voltage control without current feedback. IEEE Trans Ind Electron. 59(3), 1545–1553 (2011)
30. Yoshida, T.: Constant Current and Constant Voltage Battery Charger. Google Patents (2000)
31. Hussein, A.A.H., Batarseh, I.: A review of charging algorithms for nickel and lithium battery chargers. IEEE Trans Veh Technol. 60(3), 830–838 (2011)